Volume 27 Number 30 14 August 2025 Pages 8991-9282

Green Chemistry

Cutting-edge research for a greener sustainable future rsc.li/greenchem

Golden Mean

ISSN 1463-9262



PAPER

Yanting Wang et al.
Semi-overexpressed OsMYB86L2 specifically enhances cellulose biosynthesis to maximize bioethanol productivity by cascading lignocellulose depolymerization via integrated rapid-physical and recyclable-chemical processes



Green Chemistry



PAPER

View Article Online
View Journal | View Issue



Cite this: *Green Chem.*, 2025, **27**, 9127

Semi-overexpressed OsMYB86L2 specifically enhances cellulose biosynthesis to maximize bioethanol productivity by cascading lignocellulose depolymerization *via* integrated rapid-physical and recyclable-chemical processes†

Hailang Wang, Da,b Sufang Li,a,b Leiming Wu,a,c Weihua Zou,a Mingliang Zhang,a Youmei Wang,a,d Zhengyi Lv,a,b Peng Chen,a Peng Liu,b Yujing Yang,b Liangcai Penga,b and Yanting Wang a,b

Genetic engineering of plant cell walls has been implemented in bioenergy crops, but the tradeoff between biomass production and lignocellulose recalcitrance remains to be resolved. Although OsMYB86L2 overexpression caused a defective phenotype in a homozygous Ho86 mutant, this study found that its semi-overproduction could up-regulate cellulose biosynthesis and down-regulate non-cellulosic polymer assembly into cell walls in a heterozygous He86 mutant, which not only generated a desirable substrate that consists of a high level of cellulose and low-recalcitrance lignocellulose but also resulted in the accumulation of a much higher level of fermentable sugars (a 1.6-fold increase) with a similar grain yield to the wild type. After incubation with a recyclable alkali (CO) or organic acid (oxalic acid) and a brief (1-2 min) microwave irradiation pretreatment, the He86 mutant showed near-complete biomass saccharification from ultrasound-assistant enzymatic hydrolysis, leading to either a high yield of cellulosic ethanol (15-17% dry matter) or maximum total ethanol (25-26% dry matter) via engineered yeast fermentation. As these two optimal integrated pretreatments could largely co-extract the wall polymers to reduce cellulose polymerization and increase lignocellulose accessibility and porosity, accompanied by a distinct reduction in chemical inhibitor release, this study finally proposed a novel mechanism to elucidate how the modified lignocellulose can be completely digested and efficiently converted via integrated biomass processes, providing insights into precise lignocellulose modification and effective biomass engineering

Received 7th February 2025, Accepted 27th May 2025 DOI: 10.1039/d5gc00658a

rsc.li/greenchem

Green foundation

- 1. (1) This study generated a unique lignocellulose substrate that has increased cellulose content and reduced recalcitrance by the genetic selection of a heterozygous *He86* mutant for the first time. (2) Green-like pretreatments of the desirable lignocellulose substrate were optimally performed for remarkable depolymerization by integrating short-time (1–2 min) microwave irradiation with a recyclable alkali (CaO) or organic acid (oxalic acid). (3) Ultrasound-assistant hydrolyses were subsequently conducted to achieve near-complete biomass enzymatic saccharification.
- 2. The integrated green-like processes could effectively reduce lignocellulose recalcitrance by removing 54–72% hemicellulose and 51–59% lignin, increasing bioethanol yield by 46%, achieving recycling 66–83% of acid and alkali chemicals, and reducing chemical inhibitor release by 55%.
- 3. (1) It provides a novel genetic engineering approach for desirable lignocellulose generation. (2) Integrated rapid physical and recyclable chemical pretreatment is applicable for diverse lignocellulose substrates. (3) The simple recycling technologies remain to be explored in other acids and alkali pretreatments in the green chemistry field.

^aCollege of Plant Science & Technology, Huazhong Agricultural University, Wuhan 430070, China. E-mail: wyt@mail.hzau.edu.cn

^bKey Laboratory of Fermentation Engineering (Ministry of Education), National "111" Center for Cellular Regulation & Molecular Pharmaceutics, Hubei Key Laboratory of Industrial Microbiology, School of Life & Health Sciences, Hubei University of Technology, Wuhan, 430068, China

^cThe National Engineering Laboratory of Crop Resistance Breeding, School of Life Sciences, Anhui Agricultural University, Hefei, 230036, China ^dHouji Laboratory in Shanxi Province, Academy of Agronomy, Taiyuan, 030000, China

[†]Electronic supplementary information (ESI) available. See DOI: https://doi.org/10.1039/d5gc00658a

1. Introduction

Plant cell walls, as a characteristic carbon sink of higher plants, represent enormous lignocellulose resources that can be converted into renewable biofuels and valuable bioproducts. As plant cell walls have complicated structures to maintain plant strength and adaptation to environmental stresses, their recalcitrance poses a significant challenge for effective biomass conversion. Although genetic engineering of plant cell walls has been implemented to reduce lignocellulose recalcitrance, this simply results in a penalty to plant growth and biomass production, and thus, lignocellulose modification is limited in bioenergy crops.

As a prominent constituent of plant cell walls, cellulose biosynthesis is central to plant morphogenesis and biomass production. 11 As the cellulose synthase gene (CesA) was identified in the Atrsw1 mutant, 12,13 the overexpression of AtCesA6-like genes has been conducted to enhance both cellulose and lignin deposition into plant cell walls to achieve high-yield biomass, but lignocellulose recalcitrance is accordingly augmented in transgenic *Arabidopsis* lines. 14-16 Additionally, several families of transcription factors (TFs) for the dynamic regulation of plant secondary cell wall biosynthesis have been characterized.¹⁷ In particular, the MYB (v-myb avian myeloblastosis viral oncogene homolog) superfamily has been identified as a critical regulatory component of plant cell walls.18 The overexpression of specific MYB transcription factors, such as MYB46, MYB83, MYB58, and MYB63, has been demonstrated to induce secondary wall thickening in Arabidopsis, 19-22 whereas OsMYB103L overexpression could facilitate cellulose deposition by modulating OsCesAs and other genes associated with cellulose microfibril assembly in rice.²³ Nevertheless, the overproduction of such TFs mostly reinforced lignocellulose recalcitrance due to enriched cellulose and lignin deposition in the plant cell walls.

With respect to lignocellulose conversion, chemical pretreatments have been broadly performed as the initial step to reduce lignocellulose recalcitrance.^{2,24} Although classic acid (H2SO4, HCl) and alkali (NaOH, KOH) pretreatments are effective for the partial co-extraction of hemicellulose and lignin, the incubation of lignocellulose substrates with high concentrations of chemicals is under high temperatures is in principle required, leading to costly biomass processing along with secondary chemical waste release into the environment.²⁵⁻²⁸ Alternatively, green-like physical and chemical pretreatments have been employed, such as microwave irradiation,²⁹ intermittent ultrasonication,³⁰ liquid hot water,³¹ and recyclable chemicals.^{32,33} For instance, organic acids and CaO are increasingly considered as alternatives, due to their relatively lower corrosion and recyclable properties.34-36 Therefore, the integration of optimal physical and chemical pretreatments represents a new direction for cost-effective and green-like biomass processing. 27,37,38

Rice is a food crop cultivated worldwide with millions of tons of lignocellulose-rich straw.^{39,40} In this study, we identified a T-DNA insertion mutant in rice (*Oryza sativa*) that

exhibited greatly increased expression of OsMYB86L2 (Os05g0543600), a novel gene encoding a MYB transcription factor. We then observed defective plant growth with a great penalty to grain and biomass productivity in the homozygous mutant (termed as Ho86) that overexpressed the OsMYB86L2 gene. Unexpectedly, we observed similar plant growth and biomass yield in the heterozygous mutant (He86), which semioverexpressed OsMYB86L2, compared to its wild type. Hence, this study focused on characterization of cellulose biosynthesis in the heterozygous mutant (He86) and detected a significantly increased cellulose level and fermentable sugar accumulation along with relatively reduced contents of non-cellulosic polymers (hemicellulose, pectin, lignin). As the reduction in noncellulosic polymers accounted for improved lignocellulose recalcitrance in the He86 mutant, this study attempted to explore the optimal physical and chemical pretreatments for mature straw by integrating microwave irradiation with a recyclable organic acid (oxalic acid) or alkali (CaO). By further employing our recently-established intermittent ultrasound treatment with lignocellulose enzymatic hydrolysis, 30 this study achieved near-complete biomass saccharification in the He86 mutant, which enabled the highest yield of bioethanol via cofermentation of the released xylose and hexoses using an engineered yeast strain. 41 Finally, this study presents a novel hypothetical model to explain how the heterozygous He86 mutant is unique for enhancing cellulose biosynthesis with a related reduction in hemicellulose and lignin deposition into plant cell walls, leading to near-complete lignocellulose enzymatic saccharification and efficient bioethanol conversion, providing a powerful strategy for precise genetic engineering of lignocelluloses and effective integrated biomass processes.

2. Materials and methods

2.1. Selection of rice mutant and transgenic lines

The rice mutant was selected from an activation tag T-DNA mutagenesis pool of the japonica variety (Oryza sativa, Nipponbare/NPB). Following the isolation of flanking sequences and co-isolation identification, the mutation was characterized as a T-DNA insertion into the OsMYB86L2 gene. Transgenic rice lines were generated by utilizing a vector with an rbcS promoter for the overexpression of the full-length MYB86L2 cDNA, and the construct was then transformed into rice (NPB) calli via Agrobacterium tumefaciens strain EHA105. Positive T0 transgenic lines were selected using hygromycin (Hyg) as a selectable marker for plant transformation. The primers employed for gene cloning are detailed in Table S1.† All plants were grown in the experimental field of Huazhong Agricultural University (Wuhan, China). Dry straw tissues were powdered, passed through a 40-mesh screen (0.425 × 0.425 mm), and preserved in a dry container until in use.

2.2. RNA extraction and real-time PCR (qRT-PCR) analysis

Total RNAs were isolated from rice stem tissues at the seedling and heading stages using the Vazyme RNA Isolation Kit (R404-

1, Vazyme, Nanjing). Complementary DNA (cDNA) synthesis was carried out using the HiScript II Q RT SuperMix for qPCR (R223-01, Vazyme, Nanjing). Quantitative reverse transcription polymerase chain reaction (qRT-PCR) was conducted employing the Taq Pro Universal SYBR qPCR Master Mix (Q712-02, Vazyme, Nanjing) on a CFX384 qPCR System (Bio-Rad, USA) following the manufacturer's protocols. The obtained data were analyzed utilizing the Bio-Rad CFX Maestro software, and the $2^{-\Delta\Delta Ct}$ method was applied to calculate the relative gene expression levels. The rice housekeeping gene OsUBO (Os03g0234200) was employed as the endogenous control for normalization. The primers used in this study are detailed in Table S1.† All experiments were conducted in biological triplicate to ensure reproducibility.

2.3. RNA-seq and DAP-seq assay

Total RNAs were isolated from the stem tissues of the WT and mutants at the heading stage using the Vazyme RNA Isolation Kit (R404-1, Vazyme, Nanjing) with three biological replicates. Sequencing libraries were constructed using the TruSeq RNA Sample Preparation Kit (Illumina, San Diego, CA, USA) according to the manufacturer's protocol, and sequenced on a Hiseqplatform (Illumina). About 77686650-110159422 pairedends (36-100 bp) were generated for each sample, and raw data were subjected to quality control using FastOC and filtered using Trimmomatic from TBtools-II (v2.152) plugin.⁴² RNA-seq reads were mapped to the IRGSP-1.0 genome (https:// plants.ensembl.org/Oryza_sativa) and alignments were then assembled using the One step RNAseq 2 Expression plugin. Statistically significant differentially expressed genes (DEGs) were calculated with DESeq2 using padj < 0.01 and |log₂FoldChange| > 2.0. DEGs were annotated against the Gene Ontology enrichment analysis.

The DNA affinity purification sequencing (DAP-seq) experiments and data analysis were conducted as previously described.²³ All raw data analysis was accomplished using MACS2 GUI Wrapper CallPeaks from the TBtools-II (v2.152) plugin. 42 All enrichment peaks were visualized using IGV software (v2.19.1). The target gene was identified as the closest gene containing a peak within 2000 bp upstream of the 5'UTR.

2.4. Wall polymer extraction and assay

Plant cell wall fractionation was performed as previously described with minor modification. 43,44 The soluble sugars, lipids, starch and pectin compounds were sequentially extracted using phosphate buffer (pH 7.0), chloroform-methanol, dimethyl sulfoxide/water, and 0.5% (w/v) ammonium oxalate. The remaining crude lignocelluloses were suspended in a solution of 4 M KOH containing NaBH₄ (1.0 mg mL⁻¹) and incubated at 50 °C for 1 h. The combined supernatants (containing KOH and distilled water) were employed as the KOH-extractable hemicellulose fraction. The remaining pellets were solubilized in 72% H₂SO₄ (w/w) at 25 °C for 1 h, and the hexose was detected as the cellulose level. The total hemicellulose content was estimated by calculating the hexose and pentoses of the KOH-extractable fraction and the pentoses of the cellulose fraction. The hexose, pentose and uronic acid assays were conducted using a UV-VIS spectrometer (V-1100D, Shanghai MAPADA Instruments Co.). Total lignin was assayed according to the Laboratory Analytical Procedure of the National Renewable Energy Laboratory. 45 The alkaline lignin liquor was dried, subjected to sulfuric acid hydrolysis, and centrifuged to determine soluble compounds and acid-insoluble lignin by weight. All assays were accomplished under independent triplicates.

2.5. Cellulose staining and feature assay

Cellulose staining was conducted as described. 14 Cryosections (8 µm thickness) were meticulously cut using a microtome (RM2265, Leica). For visualization, the sections were subjected to a 3 minutes incubation with Calcofluor White M2R fluorochrome (fluorescent brightener 28; Sigma; 0.25 μg mL⁻¹ in dH₂O). Imaging was conducted using an Olympus BX-61 microscope (Japan) fitted with specific filter sets: 350/ 450 nm (ex/em) and 490/520 nm (ex/em), respectively, to visualize the stained cell walls and green emission from the FITC fluorochrome.

The crystalline cellulose was extracted with acetic acidnitric acid-water (8:1:2, v/v/v), and the crude cellulose was obtained using 4 M KOH and 8% (w/v) sodium chlorate at a pH of 4.5. The degree of polymerization (DP) of the crude cellulose and crystalline cellulose substrates were measured using the viscometry method.³¹ The intrinsic viscosity values were transformed into the cellulose DP based on the following equation:

$$DP^{0.905} = 0.75 \times [\eta] \tag{1}$$

where $[\eta]$ is the intrinsic viscosity of the solution, determined by interpolation from the USP table.

The cellulose crystalline index (CrI) was determined by the X-ray diffraction method (FRINGE CLASS ver-1.4.6.8, LANScrientific, China) as described30,46 with minor modification. Cu-Ka radiation generated at a voltage of 30 kV and current of 16 mA and a scan speed of 0.02° s⁻¹ from 10° to 60° were employed to collect diffraction data for the estimation of CrI using the equation:

$$CrI(\%) = \frac{I_{200} - I_{am}}{I_{am}} \times 100$$
 (2)

where I_{200} is the intensity of the 200 peaks at a 2θ value of around 22.5°, which represents both crystalline and amorphous materials, while I_{am} is the minimum intensity of amorphous material between the 200 and 110 peaks at 2θ around 18°.

All experiments were conducted in independent triplicates.

2.6. Oxalic acid- and CaO-microwave irradiation (MWI) pretreatments

For the oxalic acid-microwave irradiation (oxalic acid-MWI) pretreatment, a biomass sample (0.300 g) was powdered by ball milling, passed through a 40 mesh sieve, dried to a conPaper Green Chemistry

stant weight, and then incubated with 10 g of oxalic acid dihydrate (oxalic acid, 99.5%) powder and 5 mL ddH₂O in a spherical reactor. The well-mixed sample was then subjected to microwave irradiation at a power of 500 W for 1, 2, 3, or 4 min. After reaction, 50 mL of deionized water was immediately added to cool the sample. For the CaO-microwave irradiation (CaO-MWI) pretreatment, biomass powder (0.300 g) was incubated with 15 mL of a 5% CaO agueous solution (prepared using a 66.7% glycerol aqueous solution) and heated under microwave irradiation at a power of 300 W for 1, 2, 3, or 4 min. During the microwave irradiation process, magnetic stirring was employed to ensure that the biomass was well mixed, and a condensation reflux apparatus was installed to mitigate solvent evaporation losses. The pretreated lignocellulose residues were finally washed with distilled water until reaching pH 7.0 for sequential enzymatic hydrolysis. All experiments were performed under independent triplicates.

After the pretreatments, the cellulose retention, and hemicellulose and lignin removal rates were calculated according to the following equations:

Cellulose retention(%) =
$$\frac{M_{\text{GRP}}}{M_{\text{GRM}}} \times 100$$
 (3)

For this equation, $M_{\rm GPR}$ represents the mass of glucose in the pretreated residue, and $M_{\rm GRM}$ represents the mass of glucose in the raw material.

$$\mbox{Hemicellulose removal}(\%) = \left(1 - \frac{\mbox{$M_{\rm PPR}$}}{\mbox{$M_{\rm PRM}$}}\right) \times 100 \qquad (4)$$

 M_{PPR} represents the mass of pentose in pretreated residue, and M_{PRM} represents the mass of pentoses in the raw material.

$$\text{Lignin removal}(\%) = \left(1 - \frac{M_{\text{LPR}}}{M_{\text{LRM}}}\right) \times 100 \tag{5}$$

 $M_{\rm LPR}$ represents the mass of lignin in the pretreated residue, and $M_{\rm LRM}$ represents the mass of lignin in the raw material.

2.7. Recovery of oxalic acid and CaO solutions

The CaO–MWI pretreated residues were washed with a 5% (v/v) HCl solution and then agitated at 25 °C for 30 min to ensure the complete dissolution of residual CaO/Ca(OH)₂ solids. After the remaining residues were further rinsed three times with distilled water, all supernatants were centrifuged (3000 g for 5 min) to remove any remaining solid particles and an approximately 10% (m/v) Na₂CO₃ solution was added to precipitate all Ca²⁺. The resulting precipitate was filtered, washed three times with distilled water, dried in an oven at 60 °C to constant weight, and finally calcined in a muffle furnace at 900 °C for 2 h. After cooling to room temperature, the Ca²⁺ was recovered and measured.

The oxalic acid–MWI pretreated residues were washed five times with distilled water, and all supernatants were collected after centrifugation at 3000 g for 5 min. All the combined supernatants were then concentrated using an evaporator at 60 $^{\circ}$ C. Upon cooling at room temperature, the crystallized

oxalic acids were recovered by filtration. The remaining liquid was further concentrated to induce additional crystal formation, and this process was repeated until no further crystallization occurred. Finally, the obtained crystals were rinsed with a minimal amount of deionized water and dried thoroughly in a vacuum drying oven to recover the oxalic acid.

2.8. Enzymatic hydrolysis and yeast fermentation for bioethanol production

Pretreated biomass samples were washed with acetate buffer (0.2 M acetic acid-sodium acetate, pH 4.8) and then incubated with 3.2 g L⁻¹ mixed cellulases (HSB, Imperial Jade Biotechnology Co., Ltd, Ningxia 750002, China) including mixed cellulases (10.60 FPU g⁻¹ biomass) and xylanase (6.72 U g^{-1} biomass). The enzymatic hydrolysis was conducted with a 5% (w/v) solids loading for 48 h at 50 °C under 150 rpm shaking. During the enzymatic hydrolyses for 12, 24, or 36 h, ultrasonic disruption was applied for 20 min using an ultrasonic cleaner (SB-3200D, China) at a frequency of 40 kHz and an output power of 180 W. Following the enzymatic reactions, the supernatants were obtained through centrifugation at 3000g for 5 min to determine the total released sugars, including hexoses and pentoses. All the soluble sugars of the supernatants were collected for ethanol fermentation using Saccharomyces cerevisiae (Angel Yeast Co., Ltd, China) and the engineered yeast strain E4 41 as previously described. 28,46 All analyses were conducted under independent triplicates.

2.9. Detection of lignocellulose porosity and cellulose accessibility

A Micrometrics ASAP 2460 (USA) instrument was employed to assess the pore size distribution of the biomass powder as previously described. The micropore volumes were determined using the Horvath-Kawazoe (HK) and Barrett-Joyner-Halenda (BJH) methods. Cellulose accessibility was estimated by performing Congo red (CR) staining as previously described. All measurements were conducted in biological triplicates.

2.10. Fourier transform infrared (FTIR) spectroscopy scanning

FTIR spectroscopy was performed to observe the chemical groups in the rice stem samples using a PerkinElmer spectrophotometer (NEXUS 470, Thermo Fisher Scientific, Waltham, MA, USA) as previously described.⁴⁹ The FTIR spectra were acquired in absorption mode using 32 scans at a resolution of 4 cm⁻¹ within the spectral range of 4000 to 400 cm⁻¹.

2.11. Scanning electron microscopic (SEM) observation

The biomass samples were dried to a constant weight at 60 $^{\circ}$ C and then passed through a 40-mesh sieve. For microstructural characterization, the specimens were sputter-coated with gold and examined using a scanning electron microscope (SEM JSM-5610/LV, Hitachi, Tokyo, Japan). A total of 8–10 observations were conducted for each sample throughout this study.

2.12. Total organic carbon (TOC) and LC-MS/MS analyses

Total organic carbons (TOC) were determined using an automated TOC analyzer (model Vario TOC, Elementar, Germany) as described.⁵⁰ All experiments were performed in biological triplicate. For LC-MS/MS analysis, the pretreatment solution and enzymatic hydrates (0.5-1.0 mL) were accurately weighed into a centrifuge tube, diluted with twice their volume of a methanol-acetonitrile mixed solution (1:1, v/v), homogenized for 60 s, and extracted for 30 min using low-temperature ultrasonication. After centrifugation for 10 min at 12 000 rpm and 4 °C, the sample was allowed to rest for 1 h to precipitate the protein at −20 °C and then centrifuged for 10 min at 12 000 rpm and 4 °C. After the supernatants were dried under vacuum, re-dissolved using 100 µL 30% acetonitrile solution, homogenized and centrifuged for 10 min at 4 °C, the supernatants were collected for detection. The UPLC analytical conditions included a Waters HSS T3 column (100 × 2.1 mm, 1.8 μm), a temperature of 40 °C, a flow rate of 0.3 mL min⁻¹ and an injection volume of 2 µL. HRMS data were recorded using a Q Exactive HFX Hybrid Quadrupole Orbitrap mass spectrometer equipped with a heated ESI source (Thermo Fisher Scientific), utilizing the full-msddMS2 acquisition methods. The raw MS data were acquired on the Q-Exactive using Xcalibur 4.1 (Thermo Scientific), and processed using Progenesis QI (Waters Corporation, Milford, USA) software for baseline filtering, peak recognition, peak matching, retention time correction and peak alignment, resulting in a data matrix that includes retention time, mass-to-charge ratio, and peak intensity. Commercial databases and the self-built secondary mass spectrometry (MS2) database of Sanshu Biotechnology (https://www.sanshubio.com), along with their corresponding fragmentation rules, were used to identify peaks containing MS2 data. The matching of MS2 is mainly reflected in the score of the secondary fragments, where the total score is 100; a higher score indicates a more reliable identification. Generally, a score greater than 50 is considered to indicate a reliable identification.51,52 Quantified data were output in Excel format (ESI Table S7†). Data were analyzed using the R package, where they were subjected to multivariate data analysis. The specific locations of all compounds from analyzing their retention times and peak areas are described in ESI Tables 6 and 7.†

2.13. Statistical analysis

Analyses of variance (ANOVA), regression coefficients and Spearman's rank correlation coefficient were analyzed using Superior Performance Software System (SPSS version 16.0, Inc., Chicago, IL). Pair-wise comparisons were conducted between two measurements using Student's t-test. The line graph, histogram, and regression analysis for the best fit curve were plotted using Origin 8.5 software (Microcal Software, Northampton, MA). The average values were calculated from the original independent triplicate measurements for these analyses. Statistical analysis was performed using Student's

t-tests (two tail distribution and two samples with unequal variances) as *p < 0.05 and **p < 0.01.

Results and discussion 3.

3.1. Altered biomass production of homozygous and heterozygous mutants with distinct OsMYB86L2 overexpression

Employing our previously-established activating tag T-DNA mutagenesis pool for the rice variety (Nipponbare/NPB), 23 this study initially focused on identifying leaf rolling and dwarf mutation phenotypes (Fig. 1A), and then selected both homozygous and heterozygous mutants (termed as Ho86 and He86) that distinctively overexpressed the gene OsMYB86L2 (Fig. 1B-D). Through isolation of flanking sequences and co-segregation analysis, we detected that the T-DNA insertion occurred 38 bp upstream of the 5' UTR in the promoter region of Os05g0543600, and the protein homology comparison verified its gene as OsMYB86L2, an R2R3-type transcription factor (Fig. 1B). Real-time PCR assay indicated significant and distinct enhancements in the OsMYB86L2 transcription levels of the He86 and Ho86 mutants (Table S1;† Fig. 1C and D), which was validated by western blotting analysis (Fig. 1E). Compared to the wild type/WT (Nipponbare, a japonica variety), the Ho86 mutant exhibited an extreme leaf rolling and dwarf phenotype with a significant reduction (by 66%) of biomass production at the mature stage, whereas the He86 mutant exhibited only a slight reduction of 12% in biomass yield (Fig. 1F). In terms of the defective phenotype observed in the Ho86 mutant, this study further generated transgenic rice lines overexpressing the OsMYB86L2 driven with the rbcS promoter, which were verified by quantitative PCR assay and western blotting detection (Fig. S1†). Notably, the two representative transgenic lines consistently exhibited a dwarf phenotype similar to that of the Ho86 mutant, which confirmed that MYB86L2 overexpression could critically affect plant growth and development. Based on the field experiment, the Ho86 mutant had a significantly reduced grain yield per plant, while the He86 mutant had a grain yield close to that of the WT due to its significantly increased grains per panicle and seed-setting rate (Table S2†). As crop growth is strongly affected by cultivation and climate conditions, the grain yields of the rice mutants should be relatively varied in field experiments of different years.

3.2. Distinct lignocellulose compositions and soluble sugar levels of Ho86 and He86 mutants

With respect to the alteration in biomass production between the Ho86 and He86 mutants, this study determined the lignocellulose compositions of their mature rice straw (Fig. 2A). Compared to the WT, the Ho86 mutant showed a consistent reduction of 14–49% in the four wall polymers at p < 0.01levels (n = 3), whereas the *He86* mutant had a significantly increased cellulose level (by 12%) with relatively less reduction in the contents of the other three wall polymers (hemicellulose, lignin, and pectin). By performing Calcofluor stain-

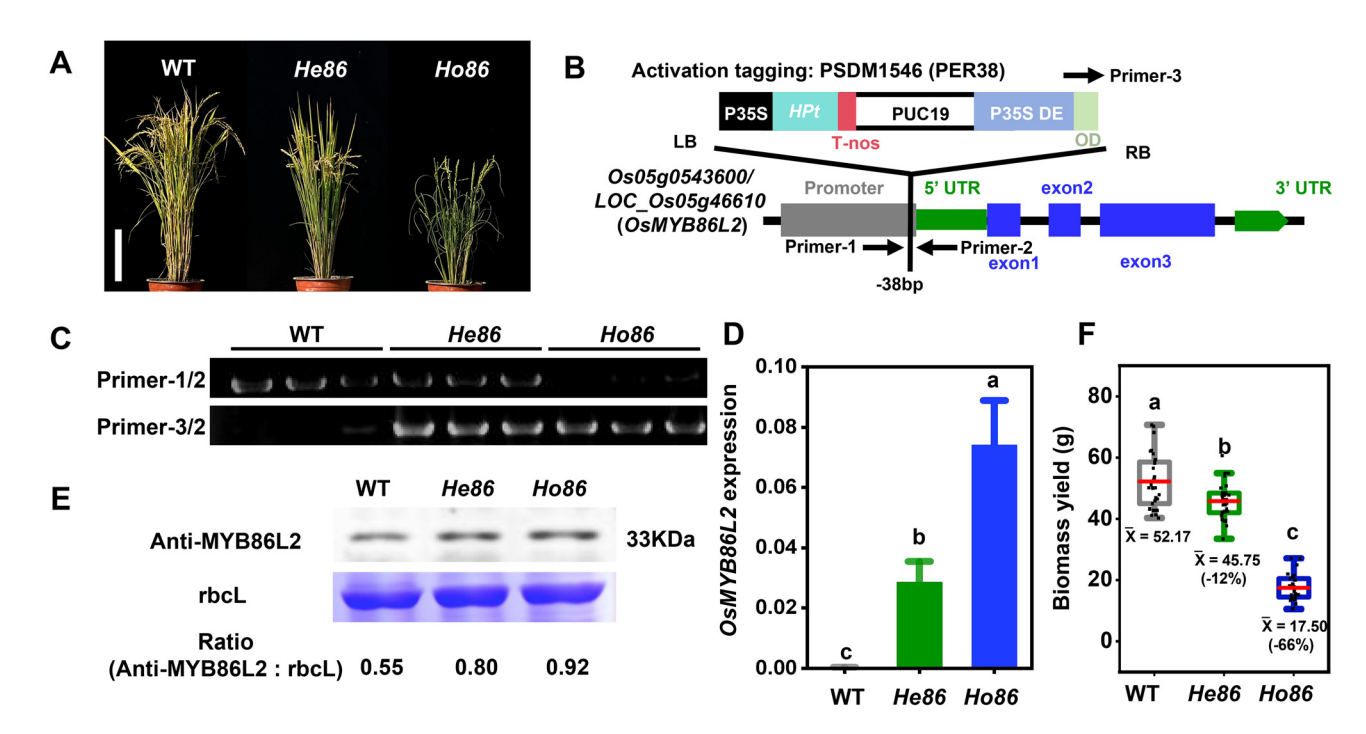


Fig. 1 Identification of He86 and Ho86 mutants. (A) Images of mature rice plants: WT/wild type ($Oryza\ sativa$, Nipponbare/NPB), He86 (heterozygous mutant) and Ho86 (homozygous mutant) (scale bar = 20 cm). (B) Identified location of the OsMYB86L2 mutation from the candidate gene Os05g0543600, with the T-DNA insertion occurring 38 bp upstream of the 5' UTR in the promoter region. (C) Genotyping of the He86 and Ho86 segregants by PCR assay. (D) Real-time PCR assay of OsMYB86L2 expression. (E) Western blotting analysis of OsMYB86L2 protein levels using anti-MYB86L2, with rbcL (rubisco large subunit protein) from the SDS gel running as an internal reference. (F) Total rice biomass at the mature stage. Data are means \pm SD ($n \ge 3$). Increase or decrease percentages (%) obtained by subtraction of the He86 mutant and WT values divided by the WT values. Lowercase letters (a, b, c) indicate multiple significant differences by the LSD test at p < 0.05, respectively.

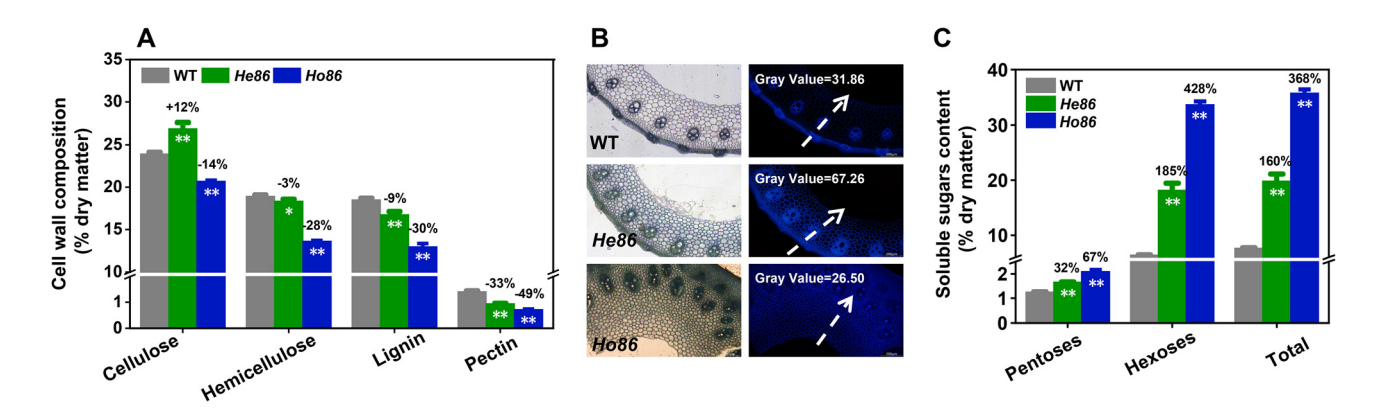


Fig. 2 Detection of lignocellulose and soluble carbohydrates of mature rice straw in He86 and Ho86 mutants. (A) Wall polymer composition. (B) Calcofluor staining of the transverse culm sections. Scale bar: 200 μ m; gray value: mean of fluorescence signal acquired through scanning along the dashed arrow. (C) Soluble sugars, data are means \pm SD (n=3). Increase or decrease percentages (%) obtained by subtraction of the He86 mutant and WT values divided by the WT values; * and ** represent significant differences between the mutant and WT by two-tailed Student's t-test at p < 0.05 and 0.01, respectively.

ing of cellulose microfibrils in the stem tissues, we observed distinct *in situ* fluorescence intensities for the *Ho86* and *He86* mutants (Fig. 2B), confirming the different cellulose levels of the two mutants relative to those of the examined WT. Despite the reduced biomass production, both mutants contained greatly increased (by 32–428%) soluble sugar levels in their mature straw, particularly in terms of hexoses (Fig. 2C), which

may be due to the excess carbohydrates from plant photosynthesis that are not utilized for wall polysaccharide syntheses. Act of the Hose mutant had even more soluble sugars than the Hose mutant (up to 2-fold more), which should be due to the much greater reduction in biomass production in the Hose mutant. The results thus suggest that OsMYB86L2 overexpression could negatively regu-

late cell wall biosynthesis for defective plant growth and reduce biomass production in the Ho86 mutant, whereas OsMYB86L2 semi-overexpression should specifically enhance cellulose biosynthesis while having a slight impact on the production of other wall polymers in the He86 mutant.

3.3. OsMYB86L2 functions as transcription factor for distinct regulation of cell wall biosynthesis

To understand the different lignocellulose compositions of the Ho86 and He86 mutants, this study searched for homologs of OsMYB86L2 from the genomes of major agricultural crops and a genetic-model plant (Arabidopsis thaliana), and three similar genes in rice were identified, namely, OsMYB86 (Os07g0634900), OsMYB86L1 (Os01g0545100) and OsMYB86L2 (Os05g0543600) (Fig. S2†). Importantly, the OsMYB86L2 gene had the highest degree of homology with ZmMYB86L2 (AQK88135) in maize, which has been defined as a major bioenergy crop with high biomass production. 48,53 Even though the MYB superfamily has been characterized as transcriptional factors for the regulation of growth and development in plants, this study also

conducted a typical transcriptional activation assay in yeast cells, and OsMYB86L2 showed a functional N-terminal transcriptional activity by predominant nuclear localization (Fig. 3A and B), which could be classified as a prototypical R2R3-type MYB transcription factor.

With respect to the MYB86L2 transcriptional levels, RNAseq was conducted using stem tissue samples of the wild type rice and mutants, and a total of 1613 differentially expressed genes (DEGs) were identified between He86 and the wild type, with 845 genes up-regulated and 768 genes down-regulated (Fig. S3†). Gene ontology enrichment analysis revealed that a significant proportion of the DEGs were associated with cell wall organization and biogenesis pathways (Fig. 3C). For the RNA-Seq analysis of the Ho86 samples, higher expression levels of MYB86L2 were observed for a greater number of DEGs (Fig. S4A†), resulting in a broader spectrum of pathways and increased enrichment in RNA modification and translationrelated processes (Fig. S4A†). In addition, the motif (C/T)(T/C) (T/C)(C/T)ACC(T/G)AC was identified as the predominant enriched sequence in MYB86L2 through DAP-seq sequencing

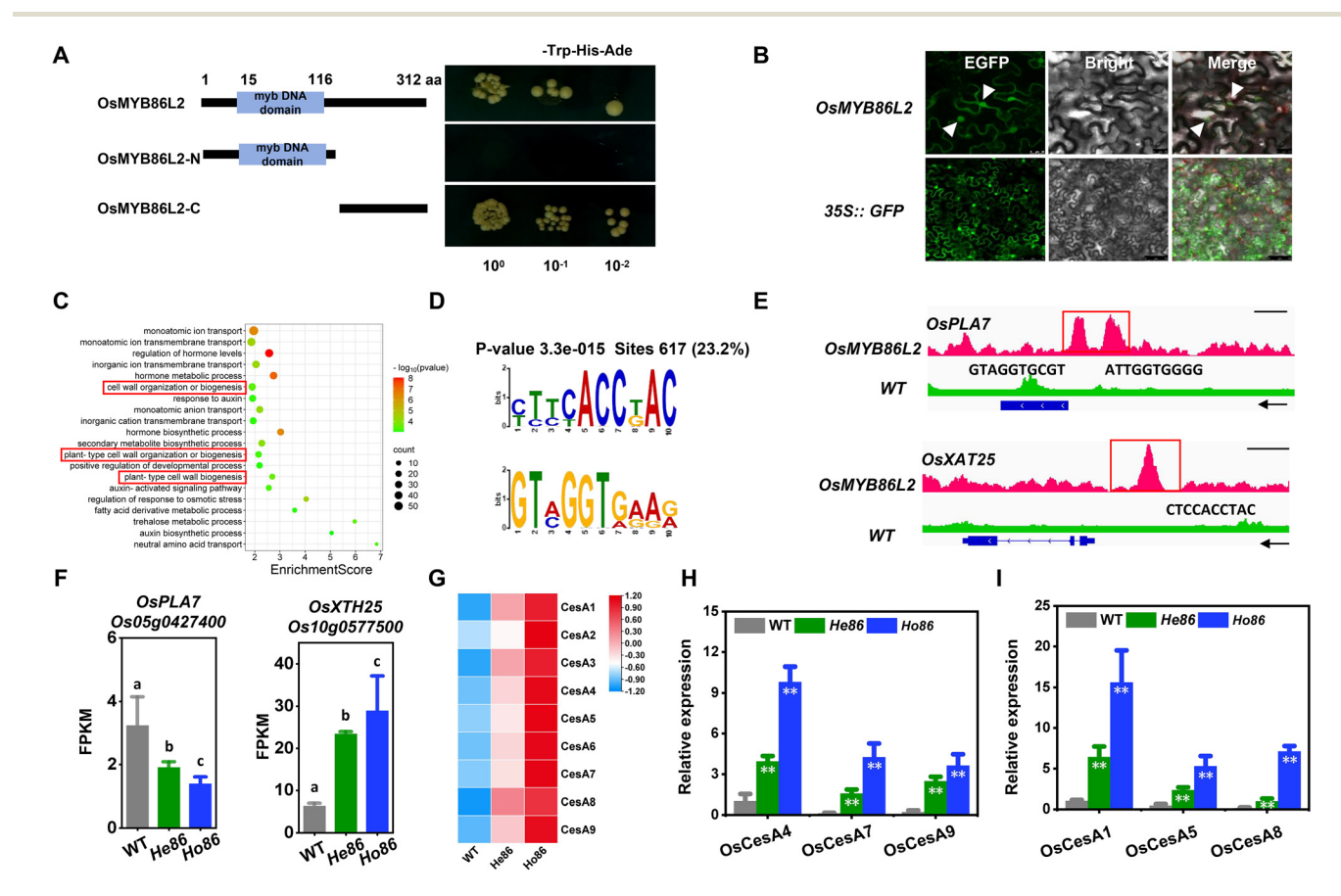


Fig. 3 Characterization of OsMYB86L2 as a transcription factor for the regulation of the gene expression of cellulose synthases (OsCesAs). (A) Transactivation analysis of different regions of OsMYB86L2 in yeast (Y187). (B) Subcellular localization of OsMYB86L2 in Nicotiana benthamiana. (C) GO analysis of differentially expressed genes obtained from RNA-seq of WT and He86 stem tissues at the heading stage. (D) Binding motifs of MYB86L2 downstream target genes identified through DAP-seq; the upper and lower rows are complementary sequences. (E) Two downstream target gene binding peaks of MYB86L2 identified through RNA-seq and DAP-seq analysis. (F) FPKM values of the two candidate target genes. (G) Heat map illustrating CesA gene expression in WT, He86, and Ho86 samples. The data were derived from RNA-seg gene counts. (H and I) Real-time PCR assay of OsCesAs genes involved in cellulose biosynthesis of secondary and primary cell walls in He86/Ho86 mutants. Data are means + SD (n = 3), ** represents significant differences between the mutant and WT by two-tailed Student's t-test at p < 0.01, respectively.

analysis (Fig. 3D). Several downstream target gene candidates for cell wall synthesis were identified (Table S3†). Notably, two genes exhibited a significant enrichment in their promoter regions, OsPAL7 (PHENYLALANINE AMMONIA-LYASE 7), a key enzyme involved in lignin synthesis, and OsXTH25 (XYLOGLUCAN ENDOTRANSGLUCOSYDASE/HYDROLASE 25), a critical enzyme for hemicellulose degradation (Fig. 3E). The changes in FPKM values paralleled the trends observed in wall polymer composition (Fig. 2A and 3F). Heat map analysis of CesAs gene expression in rice revealed that CesAs gene expression was markedly upregulated in both He86 and Ho86 (Fig. 3G). Although MYB86L2 could not directly enrich the OsCesAs promoter region, as revealed by enrichment peak analysis (Fig. S5†), real-time PCR assay of the CesAs transcription levels suggested that MYB86L2 may promote CesAs biosynthesis by indirectly regulating multiple biosynthetic pathways in plant cell walls (Fig. 3H and I). Furthermore, using public genomic data of the rice life cycle,⁵⁴ this study observed that the OsMYB86L2 gene had a similar gene expression pattern to both the OsCesA4, 7, 9 genes, in particular for the tissues (leaf sheath, stem) involved in secondary cell wall biosynthesis, and the OsCesA1, 5, 8 genes for typical tissues (ovary, embryo, endosperm) rich in primary cell walls (Fig. S6†). Taken

together, the MYB86L2 overexpression could enhance cellulose

biosynthesis in both primary and secondary cell walls, but the

Ho86 mutant showed much greater enhancement than the

He86 mutant did, leading to feedback for post-inhibited cellulose deposition in the *Ho86* mutant.

3.4. Significantly enhanced biomass saccharification to maximize bioethanol production under integrated physical and chemical processes

As the He86 mutant had a similar biomass production but an altered lignocellulose composition relative to the WT, this study focused on examining its use in enzymatic biomass saccharification for bioethanol production under integrated physical and chemical processes (Fig. 4A). For the initial biomass pretreatments, mature rice straw was incubated with either the organic acid (oxalic acid dihydrate) or recyclable alkali (5% CaO) under 500 W and 300 W microwave irradiation (MWI) treatments. Biomass saccharification was then conducted with ultrasound assistance to measure the yields of hexoses (%cellulose) released by the enzymatic hydrolyses of the pretreated lignocellulose substrates. During the time course of the pretreatments, the He86 mutant showed the highest yields of hexoses after CaO/oxalic acid-MWI pretreatment for 1 and 2 min, whereas the WT required pretreatment for 3 and 2 min (Fig. 4B). Although the He86 mutant straw had a higher cellulose level than the WT straw, it showed significantly increased yields of hexoses (by 6-21%) at p < 0.05 or 0.01 levels (n = 3) after the shorter (1-2 min) pretreatments, but the longer (3-4 min) pretreatments adversely caused much

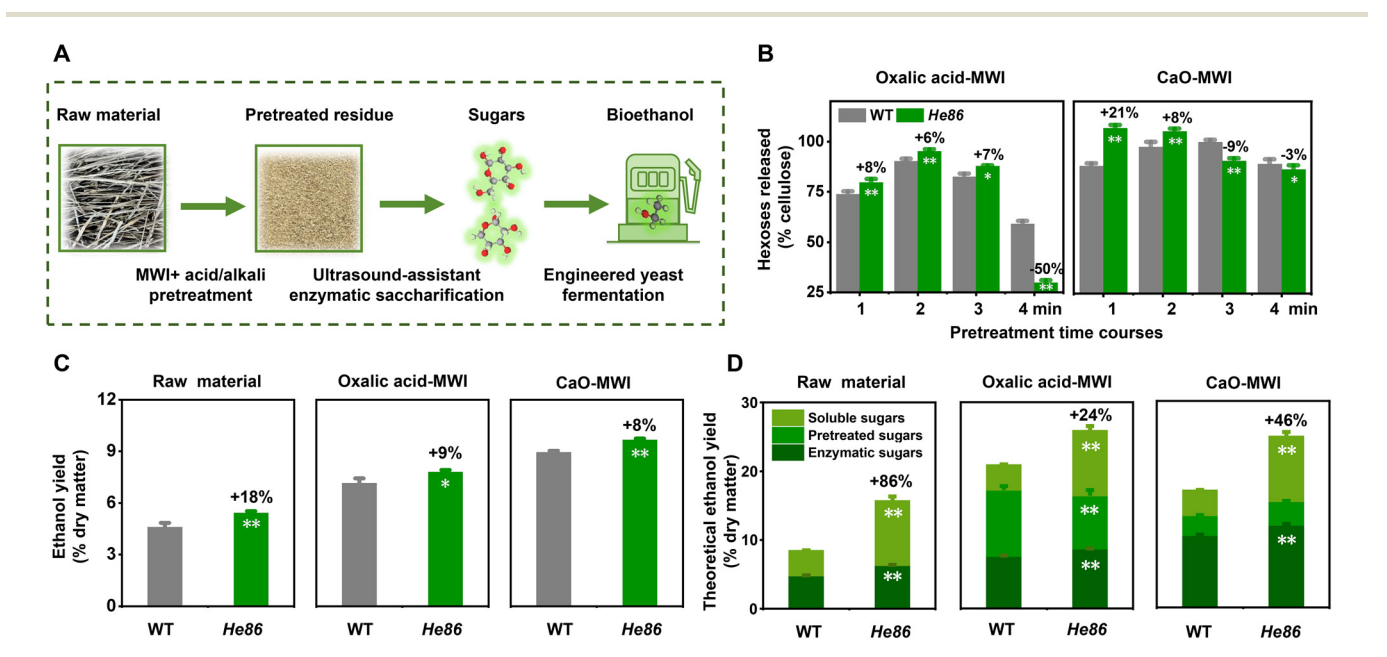


Fig. 4 Biomass saccharification and ethanol fermentation after the two optimal green-like pretreatments of mature straw of the He86 mutant and WT. (A) Experimental flow chart of the three major stages of bioethanol production. (B) Time course of the oxalic acid-microwave irradiation (MWI) and CaO-microwave irradiation (MWI) pretreatments for enhancing the hexose yields released from the enzymatic hydrolyses. (C) Bioethanol yields obtained from engineered E4 yeast fermentation using total sugars released from enzymatic hydrolysis of the raw materials and optimally pretreated (oxalic acid-MWI and CaO-MWI for 2, 1 min) residues. (D) Total theoretical ethanol yields using soluble sugars for the pretreated supernatant and enzymatic hydrates of the optimally pretreated residues. Data as mean \pm SD (n = 3), increase or decrease percentages (%) obtained by subtraction of the He86 mutant and WT values divided by the WT values. * and ** indicate significant differences between the mutant and WT by two-tailed Student's t-test at p < 0.05 and 0.01, respectively.

lower yields of hexoses in the He86 mutant, probably due to the oxidation of hexoses due to the high-concentration pretreatments. Notably, under the optimal CaO/oxalic acid-MWI pretreatment conditions (1-2 min), the He86 mutant exhibited near-complete cellulose hydrolysis with hexose yields close to 100%, indicating that these short pretreatments should be sufficient for effective biomass enzymatic saccharification in the mutant.

As a consequence, this study performed a well-established ethanol fermentation using an engineered yeast strain (E4) capable of the co-conversion of hexoses and pentose. 41 The He86 mutant achieved much greater bioethanol yields than those of the WT (by 8–18%) at p < 0.05 or 0.01 levels (n = 3) in the raw straw and optimally pretreated lignocelluloses (Fig. 4C), which should be mainly dependent on the increase in both the cellulose level and biomass enzymatic saccharification in the mutant. Mass balance calculation confirmed consistent enhancements in the saccharification and bioethanol productions achieved in the He86 mutant relative to the WT (Fig. S7†). Additionally, this work estimated the total bioethanol productivity by calculating the theoretical conversions of the three sugar sources (Fig. 4D). In general, the He86 mutant exhibited much higher bioethanol production than the WT did. In particular, the He86 mutant could reach maximum bioethanol yields of 25% and 26% (% dry matter) under the optimal CaO/oxalic acid-MWI pretreatments, whereas the WT had total bioethanol yields of only 17% and 21%. As a further comparison, compared to previously reported bioethanol productivities, 34,38,49,53,55-62 the He86 mutant achieved the highest bioethanol yields (Table 1), which should be mainly due to its much increased cellulose level and near-complete biomass enzymatic saccharification under the optimal physicalchemical pretreatments performed. In addition, using a commercial yeast strain (Angel) only capable of hexoses-ethanol conversion, significantly increased (by 27-37%) bioethanol yields were also determined in the He86 mutant relative to the WT (Fig. S8†). Therefore, the He86 mutant represents a desirable lignocellulose substrate for near-complete biomass enzymatic saccharification, enabling maximization of bioethanol productivity under integrated physical-chemical processes.

3.5. Efficient recovery and recycling of oxalic acid and CaO after optimal biomass pretreatments

Given that acid and alkali recycling aligns with the principles of green and sustainable development, this study attempted to simply recover and recycle the oxalic acid and CaO solutions remaining after the biomass pretreatments were conducted (Fig. 5). By employing a gradient concentration method, the pretreatment supernatants and residue eluents were co-evaporated to obtain approximately 66% and 71% oxalic acid crystal recoveries in the He86 mutant and wild type samples, respectively (Fig. 5A and B). Additionally, this study employed HCl to dissolve all the Ca2+ ions remaining in the pretreatment supernatant and residue, and CaCO3 was further utilized to precipitate the Ca²⁺ ions, resulting in 77% and 79% CaO recoveries in the wild type and He86 mutant samples (Fig. 5C and D). The recovered oxalic acid and CaO were further employed for the optimal CaO/oxalic acid-MWI pretreatments as conducted above, and the biomass enzymatic saccharification was determined, with hexose yields ranging from 72-83% (% cellulose) being achieved using the wild type and He86 samples (Fig. 5E and F), indicating that the restored oxalic acid and CaO are still effective for biomass pretreatment and saccharification. Hence, the optimal CaO/oxalic acid-MWI pretreatments performed in this study assure significant efficacy in the recoveries of the chemicals oxalic acid and CaO to reduce process cost and minimize environmental pollution, and their recycling efficiencies remain consistently high for further costeffective biomass saccharification.

In addition, this study calculated the green metrics corresponding to the environmental factor (E-factor).⁶³ In terms of the digestion of cellulose and its conversion into hexose and bioethanol, the He86 biomass showed relatively lower E-factors than the WT under the two optimal pretreatments conducted in this study (Table 2), which should be mainly due to either the significantly increased cellulose level and DP value or the relatively reduced cellulose CrI value in the He86 sample. Notably, the CaO-MWI pretreatment resulted in much lower E-factors than the oxalic acid-MWI one did in both the He86 and WT samples, indicating that CaO is the more desirable

Table 1 Comparison of bioethanol productivities obtained in this study and from the previous reports in rice and other crops

Plant species	Pretreatment	Solid loading (%)	Total ethanol (% dry matter)	Ref.
Rice-He86	5% CaO + MWI, 300 W, 1 min	5	25	This study
	Oxalic acid + MWI, 500 W, 2 min	5	26	·
Rice	10% CaO, 50 °C, 48 h	12	16	34
Rice	1.84% calcium hydroxide solution (100 °C, 4 h)	10	17	60
Rice	1% sulfuric acid (121 °C, 20 min) + 1% Tween-80	5	18	62
Rice	Ammonia fiber expansion	_	17	61
Rapeseed	Steam explosion + 6% H ₂ SO ₄ (120 °C, 20 min)	5	18	55
Corn	15% CaO + liquid hot water, 50 °C, 20 min	5	19	53
Sugarcane	6.4% K ₃ PO ₄ , 144.0 °C, 1 h	3.3	15	56
Cotton	Liquid hot water pretreatment (LHWP)	8	18	57
Rice	DES, MWI and laccase combinatorial pretreatment	_	21	38
Amaranth	1% NaOH, 50 °C, 2 h	5	23	59
Miscanthus	4% NaOH (50 °C, 2 h) + 1% Tween-80	5	19	49

Paper

В 100 Ε 100 recovery rate (%) +7% Hexoses released Oxalic acid 80 80 Oxalic acid recycling Oxalic acid cellulose) Pretreatment supernatant 60 60 Vacuum drying and filtration 60°C rotary 40 40 dH₂O wash evaporation % Pretreatment Washed Oxalic acid 5 times 20 20 residues and others supernatant Cooling and filtration WΤ He86 WT He86 C D F 100 CaO recovery rate (%) +12% **Hexoses released** CaO recycling 80 80 Pretreatment CaO cellulose) supernatant 60 60 900 ℃ Add 10% 40 calcination 40 Add 5% HCI Na₂CO₃ Pretreatment Washed % CaCO₂ 20 20 supernatant Shake 30 min Filtration

Fig. 5 Oxalic acid and CaO recovery and recycling from pretreatment supernatant and residues. (A and C) Experimental flow charts. (B and D) Oxalic acid and CaO recovery rates (% of total). (E and F) Hexose yields (% cellulose) released from enzymatic hydrolyses after the two optimal pretreatments were performed with the wild type and He86 mutant using the recovered oxalic acid (E) and CaO (F). Data as means \pm SD (n = 3), increase or decrease percentage (%) obtained by subtraction of the He86 mutant and WT values divided by the WT value. * and ** represent significant differences between the mutant and WT by two-tailed Student's t-test at p < 0.05 and 0.01, respectively.

Table 2 E-factor for cellulose to convert hexose and bioethanol

	CaO-MWI		Oxalic acid-MWI	
Biomass	Hexose	Bioethanol	Hexose	Bioethanol
WT	3.39	7.55	39.97	88.94
He86	2.84	4.36	30.65	47.18

green chemical for biomass processing. Despite the relatively high *E*-factor for the oxalic acid–MWI pretreatment, the application of less oxalic acid or an alternative acid remains to be explored in a future study.

3.6. Remarkable wall polymer extraction for upgraded biomass porosity from the two optimal pretreatments

To understand how the two optimal pretreatments could enhance the enzymatic biomass saccharification, this study measured the extraction rates of two major wall polymers via the pretreatments for both the He86 mutant and WT (Fig. 6A). Comparatively, the oxalic acid-MWI pretreatments could extract 72-79% of hemicelluloses and 54-59% of lignin in both the He86 mutant and WT samples, whereas the CaO-MWI pretreatments gave relatively lower polymer extraction RATES, in particular for hemicellulose removal of the WT. Using Fourier Transform infrared (FTIR) spectroscopy, we observed alterations in the characteristic peaks at 1033 and 1160 cm⁻¹ in the optimally pretreated lignocelluloses of the He86 mutant and WT (Fig. S9†), which should be attributed to the C-O-C linkages between cellulose microfibrils and hemicelluloses (Table S4†). Moreover, the pretreated-lignocelluloses displayed relatively reduced or shifted peaks at 831, 1240,

1480, 1605 and 1730⁻¹, which were assigned to C-H, C-O-C, C-H₃, C=C and C=O, accounting for lignin interlinkages with polysaccharides, respectively, which should confirm the effective extraction of hemicellulose-lignin complexes using the two optimal green-like pretreatments performed in this study.

With respect to the effective wall polymer co-extraction of the two optimal pretreatments, this study applied the Brunauer-Emmett-Teller (BET) method to measure biomass porosity, including surface area, total pore volume and pore size (Fig. 6B-D). Compared to the raw materials, the lignocelluloses exhibited overall increases in porosity after the optimally pretreatments for both the He86 mutant and WT samples, but the oxalic acid-MWI pretreatment gave much larger surface areas than the CaO-MWI pretreatment (Fig. 6B), consistent with the different extractions of wall polymers using the two pretreatments (Fig. 6A). Conversely, although the raw material of the He86 mutant showed a larger surface area (by 19%) than that of the WT, the two optimal pretreatments caused greater enlargement of the surface areas (by 47% and 101%) in the He86 mutant, mainly due to its altered lignocellulose composition (Fig. 2A). Likewise, the He86 mutant showed consistently higher total pore volumes (by 11-51%) than the WT in the raw materials and two pretreated lignocelluloses (Fig. 6C). By contrast, in average pore sizes were relatively reduced (by 6-25%) in all samples of the He86 mutant (Fig. 6D), suggesting that smaller pores should occur much more in the mutant compared to the WT. Using scanning electron microscopy, we further observed rougher surfaces for the pretreated lignocelluloses for both the He86 mutant and WT samples (Fig. 6E), which was consistent with the increased biomass porosity after the two optimal pretreatments were performed. Therefore, the

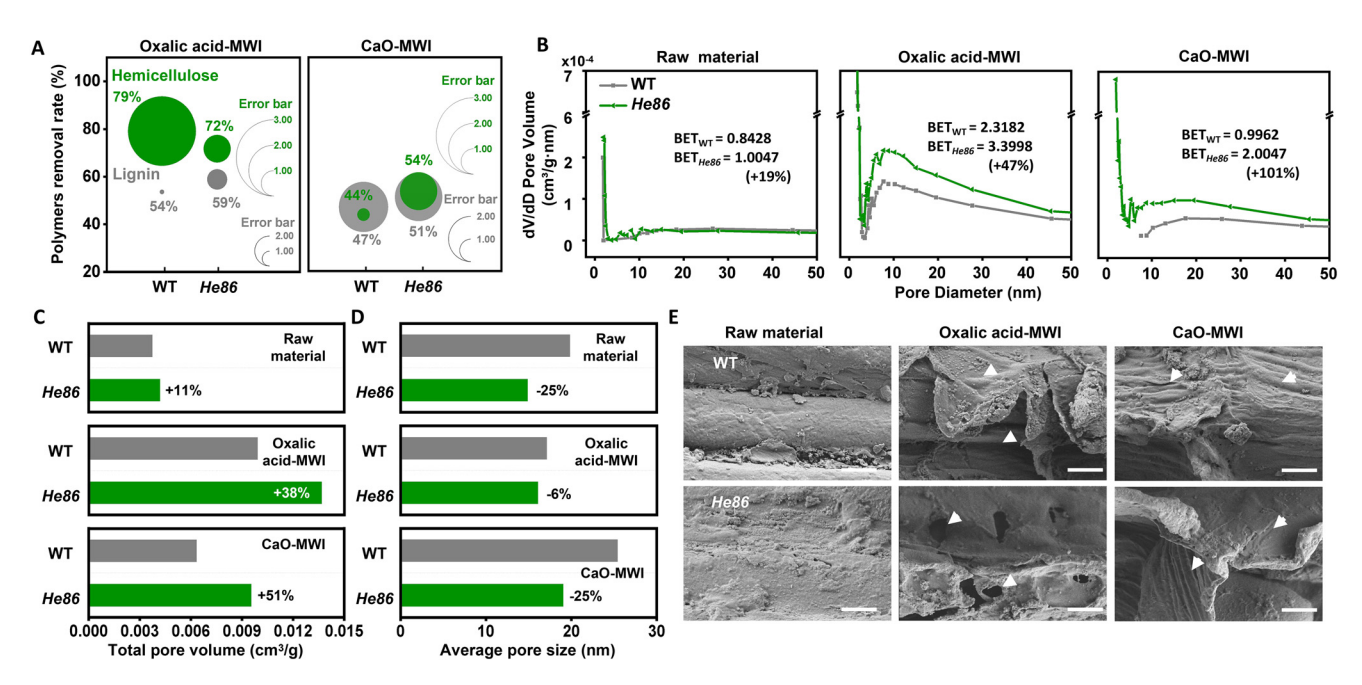


Fig. 6 Wall polymer extraction and lignocellulose porosity alteration resulting from the two optimal green-like pretreatments in the He86 mutant and WT. (A) Hemicellulose and lignin removal rates (% of total). (B) BJH pore-size distribution profiling with BET surface area ($m^2 g^{-1}$). (C and D) Total pore volume ($cm^3 g^{-1}$) and average pore size (nm, 4v/a by BET) from BET analysis. (E) SEM observation of lignocellulose substrates. Scale bars are 1 μ m and white arrows highlight the rough face with pores. Data are mean \pm SD (n = 3). Increase or decrease percentage obtained by subtraction of the mutant and WT values divided by the WT value, respectively.

two optimal pretreatments could effectively extract non-cellulosic polymers to enlarge the lignocellulose surface areas and pore volumes, particularly in the case of the *He86* mutant, which should be a major cause accounting for the greatly enhanced biomass enzymatic saccharification observed in the mutant. ^{9,64}

3.7. Consistently improved cellulose recalcitrance after the two optimal pretreatments

To further understand the near-complete cellulose hydrolysis of the He86 mutant under the two optimal pretreatments, we measured the cellulose crystalline index (CrI) and degree of polymerization (DP) in all the raw materials and pretreated lignocellulose samples. All the mutant samples showed relatively lower CrI values than those of the WT for both the raw materials and pretreated lignocelluloses (Fig. 7A). The increased CrI values in all the pretreated samples relative to the raw materials, confirmed that the two optimal pretreatments could effectively extract hemicelluloses and lignin by disassociating the wall polymer interactions by hydrogen bonds, 30,34,46 which was also consistent with the relatively greater wall polymer extraction using the conducted pretreatments (Fig. 7A). As cellulose CrI is the crucial factor negatively accounting for lignocellulose recalcitrance, 9,16,44,65 the results suggest that the He86 mutant had consistently reduced recalcitrance. Additionally, this study detected a significantly increased (by 42%) cellulose DP value in the raw material of the He86 mutant relative to the WT (Fig. 7B), which should be attributed to the greatly enhanced cellulose biosynthesis in the

mutant.^{14,66} However, the two optimal pretreatments could greatly reduce the cellulose DP values in the mutant, mainly due to the removal of a much greater amount of amorphous cellulose chains in the mutant *via* the two pretreatment processes.^{44,65} The greater amorphous cellulose extraction could also explain the slightly lower cellulose retention rates in the mutant samples relative to the WT after the two optimal pretreatment processes (Fig. 7C). This suggests that the physicochemical pretreatment may disrupt C–C and C–O bonds, leading to the co-extraction of small amounts of amorphous cellulose chains into the pretreatment liquor.

Given that cellulose DP is a key factor negatively accounting for assembly of the reducing ends of cellulose chains and cellulose nanofibrils, 44,65 this study further examined cellulose accessibility in all samples using the well-established Congo red staining method (Fig. 7D; Table S5†), which has been characterized as an integrative parameter negatively accounting for lignocellulose recalcitrance. Notably, all mutant samples showed consistently increased cellulose accessibility compared to the WT, which not only reflected the reduction in the recalcitrance of the lignocellulose of the *He86* mutant, but also confirmed the effective co-extraction of wall polymers *via* the two optimal pretreatments conducted in this study.

3.8. Decreased generation of toxic chemicals in the optimal pretreatment and enzymatic hydrolysis

As the initial pretreatment and subsequent enzymatic saccharification of biomass can generate large amounts of toxic chemicals that either inhibit final yeast fermentation or are released

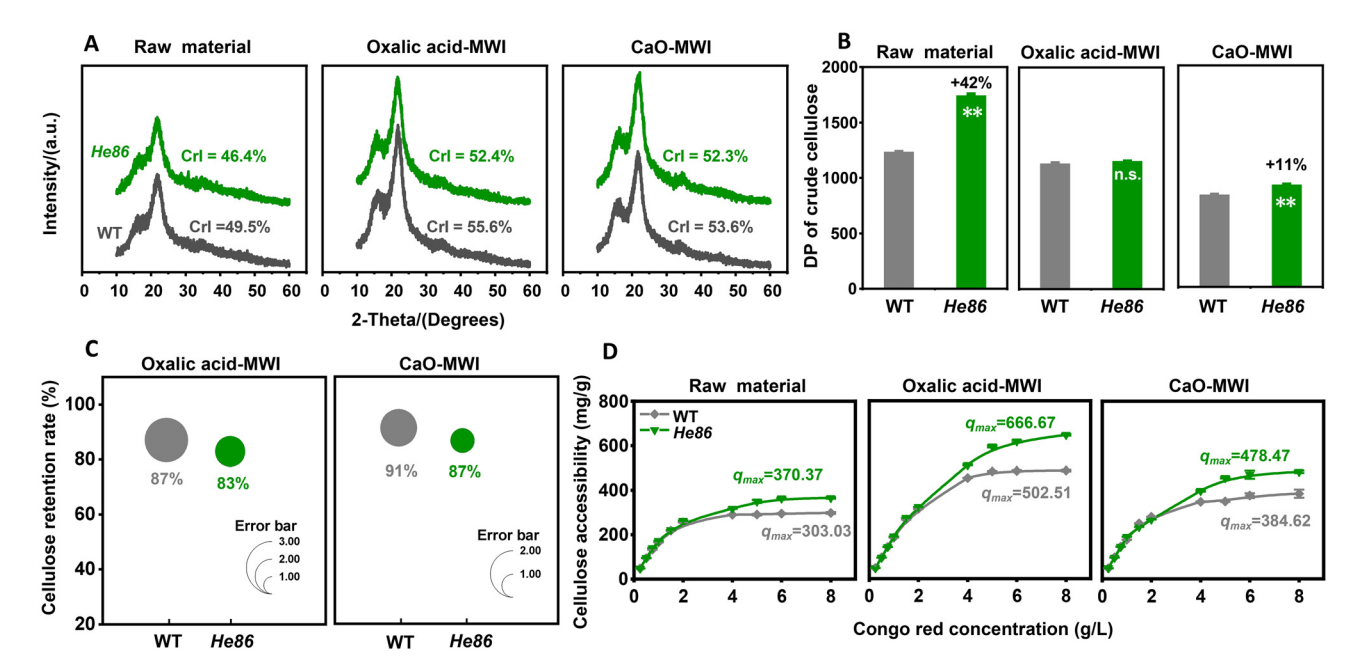


Fig. 7 Alteration of the cellulose features in the He86 mutant and WT under the two optimal green-like pretreatments. (A) Cellulose CrI (crystalline index). (B) Crude cellulose DP. (C) Cellulose retention rate. (D) Cellulose accessibility by Congo red staining with the maximum adsorption capacities (q_{max}) determined using the Langmuir isothermal adsorption model. All adsorption parameters are listed in Table S4;† Data are mean \pm SD (n=3). Increase or decrease percentage (%) obtained by subtraction of the mutant and WT values divided by the WT. ** represents significant differences between mutant and WT by two-tailed Student's t-test at the p < 0.01 level. n.s.: not significant.

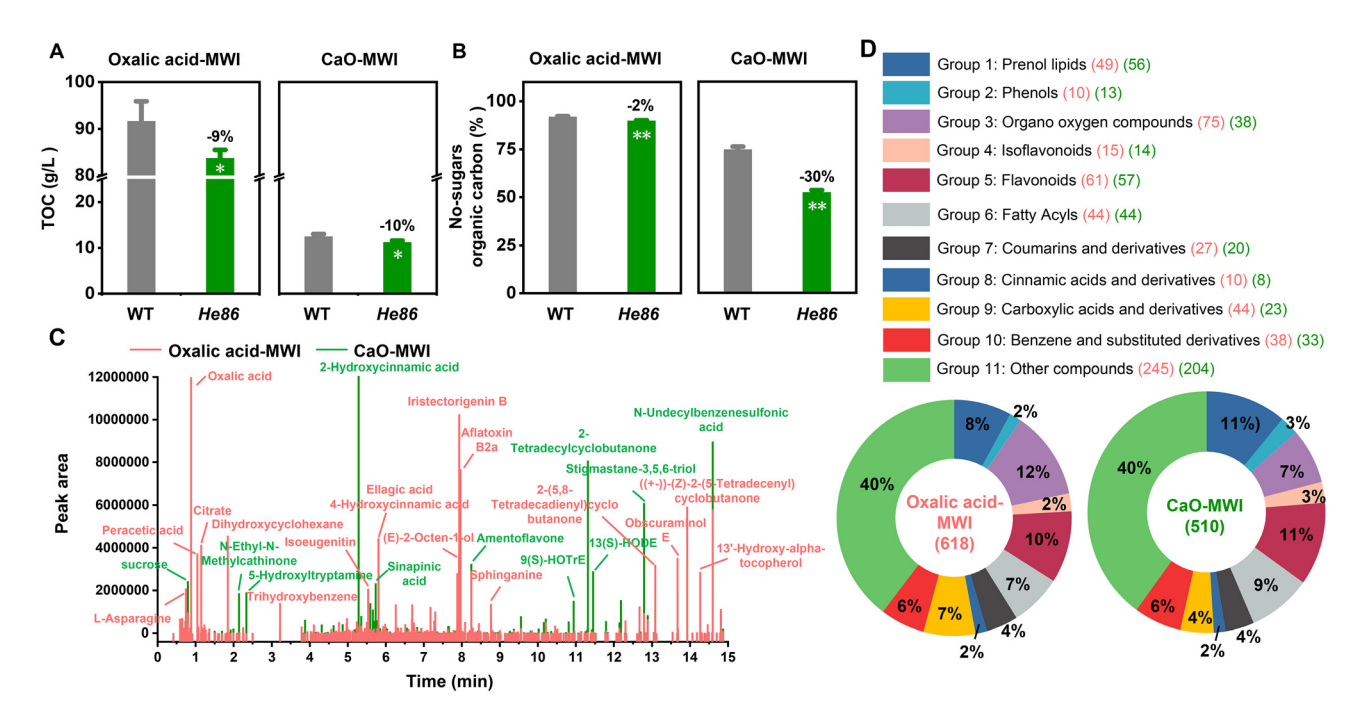


Fig. 8 Detection of chemical compounds generated from the two optimal green-like pretreatments in the He86 mutant and WT. (A) Total organic carbon (TOC) content. (B) Non-sugar organic carbon level (organic carbon excluding glucose and xylose). (C) LC-MS/MS identification of characteristic compounds. (D) Total compound groups and amounts from the two pretreatments conducted with the mutant only. Data are means \pm SD (n = 3). Increase or decrease percentage (%) obtained by subtraction of the mutant and WT value divided by the WT value. * and ** represent significant differences between the mutant and WT by two-tailed Student's t-test at p < 0.05 and 0.01, respectively.

into the environment, 27,28 this study measured all the chemical compounds generated from the two optimal pretreatments, including the total organic carbon and non-sugar organic carbon (Fig. 8A and B). In general, the CaO-MWI pretreatment produced much less total organic carbon than the oxalic acid-MWI pretreatment. In particular, the He86 mutant released significantly less chemicals than the WT did at the p < 0.05 or 0.01 level (n = 3), which should be mainly owing to the deposition of less non-cellulosic polymers into the plant cell walls with the relatively reduced lignocellulose recalcitrance in the mutant. Using mass spectrometry databases for LC-MS/MS and the scores of their secondary mass spectrometry fragments for matching, a total of 618 and 510 compounds were identified and annotated based on their peak areas and reten-

tion times, revealing the different compound compositions in the two pretreatment supernatants (Fig. 8C). We further categorized the identified the compounds into 11 groups based on their chemical properties and functional groups (Fig. 8D). Comparatively, the CaO-MWI pretreatment generated many fewer types of organo-oxygen compounds (Group 3), carboxylic acids and derivatives (Group 9) and other compounds (Group 11) than the oxalic acid-MWI pretreatment, which should be mainly due to the significantly reduced compounds from the CaO-MWI pretreatment. Additionally, this study detected much lower total organic carbon (by 10-fold) levels after the subsequent enzymatic hydrolyses of the pretreated lignocelluloses, with the He86 mutant releasing fewer compounds, particularly for the enzymatic hydrolysis of the CaO-MWI pre-

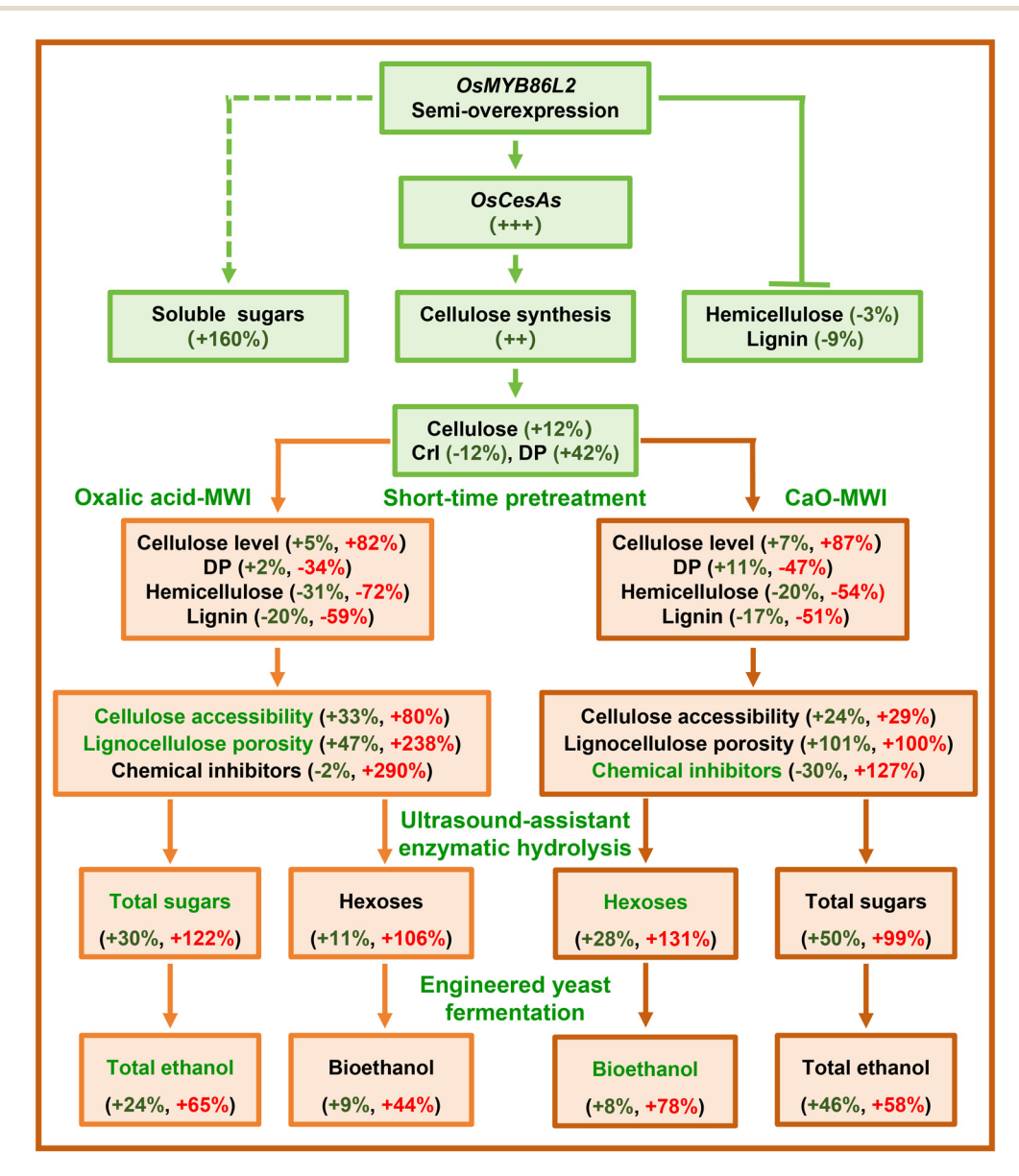


Fig. 9 Hypothetical model to link the major parameters accounting for the how genetic-modified lignocellulose of He86 mutant is digested and converted under the two optimal green-like pretreatments. Green (+) represents a factor that is improved in the mutant relative to the WT. Red (+) represents a factor that is enhanced from pretreatment, enzymatic hydrolysis or yeast fermentation in the mutant.

Paper

treated lignocellulose (Fig. S10A and 10B†). Likewise, a total of 11 groups of chemicals were also detected in the enzymatic hydrates (Fig. S10C and S11; Table S6†), but the enzymatic liquid of the CaO-MWI pretreated lignocellulose produced relatively fewer compounds only in Groups 10 & 11 (Fig. S10C†) compared to the pretreatment supernatant (Fig. 8D). Overall, the He86 mutant produced significantly fewer toxic chemical compounds in the two optimal pretreatments and sequential enzymatic hydrolyses, which represents another reason for the greatly enhanced biomass enzymatic saccharification and final veast fermentation capacity of the mutant.

3.9. A hypothetical model for the enhanced biomass saccharification and bioethanol productivity

Based on all the major findings achieved in this study, a mechanistic model was proposed to elucidate how the integrated green-like biotechnology achieves the near-complete enzymatic saccharification to maximize bioethanol productivity in the He86 mutant (Fig. 9). Although overexpression of the MYBs family has increased biomass production in most transgenic plants examined, it also increases the lignocellulose recalcitrance against enzymatic biomass saccharification. 21,67 In this work, semi-overexpression of OsMYB86L2 specifically upregulated cellulose biosynthesis to enhance cellulose deposition into plant cell walls by increasing the expression of various OsCesAs in the He86 mutant. Unexpectedly, this study also determined significantly reduced cellulose CrI values and non-cellulosic polymer (hemicellulose, lignin) levels that could account for the relatively improved lignocellulose recalcitrance in the He86 mutant, which was quite different from previous reports in other transgenic plants. Despite the reduced lignocellulose recalcitrance from distinct site mutations of OsCesAs, 9,34,44 almost all mutants have shown both less cellulose and more lignin deposition to maintain the mechanical strength and biomass production of the plant, which represents another difference from the He86 mutant. Moreover, as the He86 mutant accumulated much greater amounts of soluble sugars that could be directly fermented for bioethanol production, OsMYB86L2 semi-overexpression should consequently regulate carbon partitioning from the deposition of distinct wall polysaccharides. 14,68 Enhanced cellulose biosynthesis can cause a high accumulation of long-DP cellulose microfibrils in transgenic plants; 14,16 this study also determined a higher cellulose DP value in the He86 mutant, but the two optimal physical-chemical pretreatments could greatly reduce its cellulose DP value to a level close to that of the WT, probably due to the effective extraction of amorphous cellulose chains. 9,44 Notably, the two optimal pretreatments remarkably co-extracted hemicelluloses and lignin to upgrade cellulose accessibility and lignocellulose porosity, which was responsible for the greatly improved lignocellulose recalcitrance in the mutant. This enabled an integrative enhancement of the ultrasound-assisted enzymatic hydrolysis for near-complete biomass saccharification in the mutant. Nevertheless, even though the CaO-MWI pretreatment extracted relatively less wall polymers than the oxalic acid-MWI pretreatment did, it

produced fewer chemical inhibitors, thus sustaining the high biomass saccharification and bioethanol production. Conversely, more total sugars were obtained from the oxalic acid-MWI pretreatment and sequential enzymatic hydrolysis, resulting in the achievement of a higher yield of total bioethanol in the mutant. Therefore, this model has demonstrated an integrative strategy for near-complete selective enzymatic biomass saccharification and thus high-vield bioethanol productivity via the precise engineering of plant cell walls coupled with two optimal biomass processes.

Conclusion

While OsMYB86L2 overexpression can seriously affect plant growth and biomass production, this study has found that its semi-overproduction specifically enhances cellulose biosynthesis and consequently reduces the deposition of other wall polymers into cell walls while not affecting plant growth and biomass production, which leads to a "three birds with one stone" effect for generating a desirable substrate with a high level of cellulose and low-recalcitrance lignocellulose in the heterozygous He86 mutant. These findings are fairly different from those for previously reported transgenic plants and genetic mutants, and allow the achievement of near-complete biomass enzymatic saccharification to maximize bioethanol productivity after conducting the two optimal CaO-MWI and oxalic acid-MWI pretreatments for very short times. Notably, this study achieved relatively high recovery and recycling of the CaO and oxalic acid after the two optimal pretreatments were performed. The CaO-MWI pretreatment was advantageous for the low-E-factor conversion of cellulose into bioethanol, while the oxalic acid-MWI treatment produced relatively more total bioethanol from the fermentation of all soluble sugars using an engineered yeast strain. Hence, this study has proposed a novel mechanism to link all the major findings regarding the degradability and transformability of the desirable lignocellulose, providing a green-like strategy for effectively integrating up-stream lignocellulose modification and down-cascade biomass conversion.

Author contributions

Hailang Wang: Investigation, methodology, formal analysis, writing - original draft. Sufang Li: Methodology, formal analysis, investigation. Leiming Wu: Methodology, formal analysis. Weihua Zou: Methodology, formal analysis. Mingliang Zhang: Methodology, formal analysis. Youmei Wang: Methodology, formal analysis. Zhengyi Lv: Formal analysis, methodology. Peng Chen: Writing - review & editing, validation. Peng Liu: Formal analysis, methodology. Yujing Yang: Methodology, investigation, validation. Liangcai Peng: Conceptualization, supervision, funding acquisition. Yanting Wang: Conceptualization, writing - review & editing, supervision, funding acquisition.

Data availability

The author of the manuscript "Semi-overexpressed OsMYB86L2 specifically enhances cellulose biosynthesis to maximize bioethanol productivity by cascading lignocellulose depolymerization via integrated rapid-physical and recyclable-chemical processes" confirms that the data supporting the findings of this study is available within the article.

Conflicts of interest

The authors declare that they have no known competing financial interests or personal relationships that could have appeared to influence the work reported in this paper.

Acknowledgements

This work was supported by the National Natural Science Foundation of China (32470273, 32101701), Hubei Provincial Natural Science Foundation of China for Excellent Young Scientists (2024AFA100), National 111 Project of Ministry of Education of China (BP0820035), the Initiative Grant of Hubei University of Technology for High-level Talents (GCC20230001).

References

- W. Li, Y. Lin, Y. L. Chen, C. G. Zhou, S. Li, N. De Ridder,
 D. M. Oliveira, L. J. Zhang, B. C. Zhang, J. P. Wang,
 C. Z. Xu, X. K. Fu, K. M. Luo, A. M. Wu, T. Demura,
 M. Z. Lu, Y. H. Zhou, L. G. Li, T. Umezawa, W. Boerjan and
 V. L. Chiang, *Mol. Plant*, 2024, 17, 112–140.
- 2 R. Zhang, H. R. Gao, Y. T. Wang, B. He, J. Lu, W. B. Zhu, L. C. Peng and Y. T. Wang, *Bioresour. Technol.*, 2023, 369, 128315.
- 3 D. J. Cosgrove, Nat. Rev. Mol. Cell Biol., 2024, 25, 340-358.
- 4 L. Vaahtera, J. Schulz and T. Hamann, *Nat. Plants*, 2019, 5, 924–932.
- 5 S. Wolf, Annu. Rev. Plant Biol., 2022, 73, 323-353.
- 6 E. Q. Tavares, A. P. De Souza and M. S. Buckeridge, *J. Exp. Bot.*, 2015, **66**, 4133–4143.
- 7 C. H. Ha, X. L. Rao, G. Saxena and R. A. Dixon, New Phytol., 2021, 231, 60–74.
- 8 Y. T. Wang, C. F. Fan, H. Z. Hu, Y. Li, D. Sun, Y. M. Wang and L. C. Peng, *Biotechnol. Adv.*, 2016, 34, 997–1017.
- 9 R. Zhang, Z. Hu, H. Peng, P. Liu, Y. Wang, J. Li, J. Lu, Y. Wang, T. Xia and L. Peng, *Green Chem.*, 2023, 25, 1096– 1106.
- 10 H. Yu, G. F. Zhang, J. Y. Liu, P. Liu, H. Peng, Z. P. Teng, Y. Li, X. F. Ren, C. X. Fu, J. F. Tang, M. Li, Y. T. Wang, L. Q. Wang and L. P. Peng, J. Adv. Res., 2025, DOI: 10.1016/ j.jare.2025.01.048.
- 11 G. B. Pedersen, L. Blaschek, K. E. H. Frandsen, L. C. Noack and S. Persson, *Mol. Plant*, 2023, **16**, 206–231.

- 12 T. Arioli, L. C. Peng, A. S. Betzner, J. Burn, W. Wittke, W. Herth, C. Camilleri, H. Höfte, J. Plazinski, R. Birch, A. Cork, J. Glover, J. Redmond and R. E. Williamson, *Science*, 1998, 279, 717–720.
- 13 L. C. Peng, Y. Kawagoe, P. Hogan and D. Delmer, *Science*, 2002, 295, 147–150.
- 14 H. Z. Hu, R. Zhang, S. Q. Feng, Y. M. Wang, Y. T. Wang, C. F. Fan, Y. Li, Z. Y. Liu, R. Schneider, T. Xia, S. Y. Ding, S. Persson and L. C. Peng, *Plant Biotechnol. J.*, 2018, 16, 976–988.
- 15 H. Z. Hu, R. Zhang, Z. S. Tao, X. K. Li, Y. Li, J. F. Huang, X. X. Li, X. Han, S. Q. Feng, G. M. Zhang and L. C. Peng, Plant Cell Physiol., 2018, 59, 1144–1157.
- 16 Y. H. Ai, H. L. Wang, P. Liu, H. Yu, M. D. Sun, R. Zhang, J. F. Tang, Y. T. Wang, S. Q. Feng and L. C. Peng, *Sci. Bull.*, 2024, 69, 3815–3819.
- M. Taylor-Teeples, L. Lin, M. De Lucas, G. Turco,
 T. W. Toal, A. Gaudinier, N. F. Young, G. M. Trabucco,
 M. T. Veling, R. Lamothe, P. P. Handakumbura, G. Xiong,
 C. Wang, J. Corwin, A. Tsoukalas, L. Zhang, D. Ware,
 M. Pauly, D. J. Kliebenstein, K. Dehesh, I. Tagkopoulos,
 G. Breton, J. L. Pruneda-Paz, S. E. Ahnert, S. A. Kay,
 S. P. Hazen and S. M. Brady, Nature, 2015, 517, 571-575.
- 18 R. Q. Zhong, C. Lee, J. L. Zhou, R. L. Mccarthy and Z. H. Ye, *Plant Cell*, 2008, **20**, 2763–2782.
- 19 J. H. Ko, W. C. Kim and K. H. Han, *Plant J.*, 2009, **60**, 649–665.
- 20 J. H. Ko, H. W. Jeon, W. C. Kim, J. Y. Kim and K. H. Han, Ann. Bot., 2014, 114, 1099–1107.
- 21 R. L. Mccarthy, R. Zhong and Z. H. Ye, *Plant Cell Physiol.*, 2009, **50**, 1950–1964.
- 22 J. L. Zhou, C. H. Lee, R. Q. Zhong and Z. H. Ye, *Plant Cell*, 2009, 21, 248–266.
- 23 L. M. Wu, M. L. Zhang, R. Zhang, H. Z. Yu, H. L. Wang, J. Y. Li, Y. M. Wang, Z. Hu, Y. T. Wang, Z. Luo, L. Li, L. Q. Wang, L. C. Peng and T. Xia, *Biotechnol. Biofuels*, 2021, 14, 245.
- 24 S. N. Sun, S. L. Sun, X. F. Cao and R. C. Sun, *Bioresour. Technol.*, 2016, 199, 49–58.
- 25 C. F. Fan, H. Yu, S. F. Qin, Y. L. Li, A. Alam, C. Z. Xu, D. Fan, Q. W. Zhang, Y. T. Wang, W. B. Zhu, L. C. Peng and K. M. Luo, *Biotechnol. Biofuels*, 2020, 13, 9.
- 26 S. L. Si, Y. Chen, C. F. Fan, H. Z. Hu, Y. Li, J. F. Huang, H. F. Liao, B. Hao, Q. Li, L. C. Peng and Y. Y. Tu, *Bioresour. Technol.*, 2015, 183, 248–254.
- 27 Y. M. Wang, P. Liu, G. F. Zhang, Q. M. Yang, J. Lu, T. Xia, L. C. Peng and Y. T. Wang, Renewable Sustainable Energy Rev., 2021, 137, 110586.
- 28 M. Li, S. L. Si, B. Hao, Y. Zha, C. Wan, S. F. Hong, Y. B. Kang, J. Jia, J. Zhang, M. Li, C. Q. Zhao, Y. Y. Tu, S. G. Zhou and L. C. Peng, *Bioresour. Technol.*, 2014, 169, 447–454.
- 29 H. Q. Li, Y. S. Qu, Y. Q. Yang, S. L. Chang and J. Xu, *Bioresour. Technol.*, 2016, **199**, 34–41.
- 30 Z. Hu, Q. Li, Y. Y. Chen, T. Q. Li, Y. M. Wang, R. Zhang, H. Peng, H. L. Wang, Y. T. Wang, J. F. Tang, M. N. Aftab and L. C. Peng, *Bioresour. Technol.*, 2023, 369, 128437.

Paper

31 M. Hu, H. Yu, Y. Li, A. Li, Q. M. Cai, P. Liu, Y. Y. Tu, Y. T. Wang, R. F. Hu, B. Hao, L. C. Peng and T. Xia, Carbohydr. Polym., 2018, 202, 434–443.

- 32 Z. Usmani, M. Sharma, P. Gupta, Y. Karpichev, N. Gathergood, R. Bhat and V. K. Gupta, *Bioresour. Technol.*, 2020, **304**, 123003.
- 33 Z. K. Wang, H. Li, X. C. Lin, L. Tang, J. J. Chen, J. W. Mo, R. S. Yu and X. J. Shen, *Bioresour. Technol.*, 2020, 307, 123237.
- 34 Y. H. Ai, S. Q. Feng, Y. M. Wang, J. Lu, M. D. Sun, H. Z. Hu, Z. Hu, R. Zhang, P. Liu, H. Peng, Y. T. Wang, L. M. Cao, T. Xia and L. C. Peng, *Ind. Crops Prod.*, 2021, 173, 114133.
- 35 B. G. Cheng, X. Zhang, Q. X. Lin, F. X. Xin, R. C. Sun, X. H. Wang and J. L. Ren, Biotechnol. Biofuels, 2018, 11, 324
- 36 K. K. Valladares-Diestra, L. Porto De Souza Vandenberghe, L. A. Zevallos Torres, A. Zandoná Filho, A. Lorenci Woiciechowski and C. Ricardo Soccol, *Bioresour. Technol.*, 2022, 343, 126074.
- 37 R. G. Saratale, V. K. Ponnusamy, G. Piechota, B. Igliński, S. Shobana, J. H. Park, G. D. Saratale, H. S. Shin, J. R. Banu, V. Kumar and G. Kumar, *Bioresour. Technol.*, 2023, 387, 129560.
- 38 D. Sawhney, S. Vaid, R. Bangotra, S. Sharma, H. C. Dutt, N. Kapoor, R. Mahajan and B. K. Bajaj, *Bioresour. Technol.*, 2023, 375, 128791.
- 39 P. Binod, R. Sindhu, R. R. Singhania, S. Vikram, L. Devi, S. Nagalakshmi, N. Kurien, R. K. Sukumaran and A. Pandey, *Bioresour. Technol.*, 2010, 101, 4767–4774.
- 40 W. W. Zhang, X. Y. Xu, Y. J. Yuan and Z. C. Wang, Front. Chem. Sci. Eng., 2023, 11, 1225073.
- 41 B. Y. He, B. Hao, H. Z. Yu, F. Tu, X. Y. Wei, K. Xiong, Y. J. Zeng, H. Zeng, P. Liu, Y. Y. Tu, Y. T. Wang, H. Kang, L. C. Peng and T. Xia, *Renewable Energy*, 2022, **186**, 341–349.
- 42 C. J. Chen, Y. Wu, J. W. Li, X. Wang, Z. H. Zeng, J. Xu, Y. L. Liu, J. T. Feng, H. Chen, Y. H. He and R. Xia, *Mol. Plant*, 2023, 16, 1733–1742.
- 43 L. C. Peng, C. H. Hocart, J. W. Redmond and R. E. Williamson, *Planta*, 2000, **211**, 406–414.
- 44 R. Zhang, Z. Hu, Y. T. Wang, H. Z. Hu, F. C. Li, M. Li, A. Ragauskas, T. Xia, H. Y. Han, J. F. Tang, H. Z. Yu, B. Q. Xu and L. C. Peng, *Nat. Commun.*, 2023, 14, 1100.
- 45 A. Sluiter, B. Hames, R. Ruiz, C. Scarlata, J. Sluiter, D. Templeton and D. Crocker, Determination of structural carbohydrates and lignin inbiomass, NREL/TP-510-42618, 2008.
- 46 F. C. Li, G. S. Xie, J. F. Huang, R. Zhang, Y. Li, M. L. Zhang, Y. T. Wang, A. Li, X. K. Li, T. Xia, C. C. Qu, F. Hu, A. J. Ragauskas and L. C. Peng, *Plant Biotechnol. J.*, 2017, 15, 1093–1104.
- 47 L. L. Cheng, L. Q. Wang, L. Y. Wei, Y. Wu, A. Alam, C. B. Xu, Y. T. Wang, Y. Y. Tu, L. C. Peng and T. Xia, *Green Chem.*, 2019, 21, 3693–3700.
- 48 T. Q. Li, H. Peng, B. Y. He, C. Y. Hu, H. Y. Zhang, Y. N. Li, Y. J. Yang, Y. T. Wang, M. A. Bakr, M. Z. Zhou,

- L. C. Peng and H. Kang, Int. J. Biol. Macromol., 2024, 264, 130448.
- 49 A. Alam, R. Zhang, P. Liu, J. F. Huang, Y. T. Wang, Z. Hu, M. Madadi, D. Sun, R. F. Hu, A. Ragauskas, Y. Y. Tu and L. C. Peng, *Biotechnol. Biofuels*, 2019, 12, 99.
- 50 Y. T. Wang, H. Y. Zhang, Y. N. Li, H. Yu, D. Sun, Y. J. Yang, R. Zhang, L. Yu, F. Ma, M. N. Aftab, L. C. Peng and Y. T. Wang, *Int. J. Biol. Macromol.*, 2025, 291, 138865.
- 51 Q. Q. Yang, X. F. Mei, Z. R. Wang, X. H. Chen, R. Zhang, Q. L. Chen and J. Q. Kan, *Food Chem.*, 2021, 347, 129085.
- 52 S. Alseekh, A. Aharoni, Y. Brotman, K. Contrepois, J. D'auria, J. Ewald, J. C. Ewald, P. D. Fraser, P. Giavalisco, R. D. Hall, M. Heinemann, H. Link, J. Luo, S. Neumann, J. Nielsen, L. Perez De Souza, K. Saito, U. Sauer, F. C. Schroeder, S. Schuster, G. Siuzdak, A. Skirycz, L. W. Sumner, M. P. Snyder, H. Tang, T. Tohge, Y. Wang, W. Wen, S. Wu, G. Xu, N. Zamboni and A. R. Fernie, Nat. Methods, 2021, 18, 747–756.
- 53 L. M. Wu, S. Q. Feng, J. Deng, B. Yu, Y. M. Wang, B. Y. He, H. Peng, Q. Li, R. F. Hu and L. C. Peng, *Green Chem.*, 2019, 21, 4388–4399.
- 54 Y. Sato, H. Takehisa, K. Kamatsuki, H. Minami, N. Namiki, H. Ikawa, H. Ohyanagi, K. Sugimoto, B. A. Antonio and Y. Nagamura, *Nucleic Acids Res.*, 2013, 41, D1206–D1213.
- 55 J. Deng, X. B. Zhu, P. Chen, B. Y. He, S. W. Tang, W. Y. Zhao, L. X. Li, R. Zhang, Z. Y. Lv, H. Kang, L. Yu and L. C. Peng, Sustainable Energy Fuels, 2020, 4, 607–618.
- 56 Y. S. Fu, H. R. Gao, H. Yu, Q. M. Yang, H. Peng, P. Liu, Y. Q. Li, Z. Hu, R. Zhang, J. Y. Li, Z. Qi, L. Q. Wang, L. C. Peng and Y. T. Wang, *Renewable Energy*, 2022, 200, 1371–1381.
- 57 W. Jiang, S. Chang, H. Q. Li, P. Oleskowicz-Popiel and J. Xu, *Bioresour. Technol.*, 2015, **176**, 175–180.
- 58 Y. Li, P. Liu, J. Huang, R. Zhang, Z. Hu, S. Feng, Y. Wang, L. Wang, T. Xia and L. Peng, *Green Chem.*, 2018, 20, 2047– 2056.
- 59 M. Madadi, Y. M. Wang, R. Zhang, Z. Hu, H. R. Gao, D. Zhan, H. Yu, Q. M. Yang, Y. T. Wang, Y. Y. Tu, T. Xia and L. C. Peng, *Ind. Crops Prod.*, 2022, 177, 114471.
- 60 R. Nunta, C. Techapun, S. Sommanee, C. Mahakuntha, K. Porninta, W. Punyodom, Y. Phimolsiripol, P. Rachtanapun, W. Wang, X. S. Zhuang, W. Qi, K. Jantanasakulwong, A. Reungsang, A. A.-O. Kumar and N. A.-O. Leksawasdi, *Sci. Rep.*, 2023, 13, 727.
- 61 C. Zhong, M. W. Lau, V. Balan, B. E. Dale and Y. Yuan, *Appl. Microbiol. Biotechnol.*, 2009, **84**, 667–676.
- 62 Y. Y. Li, J. D. Zhuo, P. Liu, P. Chen, H. Z. Hu, Y. M. Wang, S. G. Zhou, Y. Y. Tu, L. C. Peng and Y. T. Wang, *Carbohydr. Polym.*, 2018, 192, 273–281.
- 63 R. A. Sheldon, *Green Chem.*, 2017, **19**, 18–43.
- 64 A. Alam, Y. M. Wang, F. Liu, H. Kang, S. W. Tang, Y. T. Wang, Q. M. Cai, H. L. Wang, H. Peng, Q. Li, Y. Zeng, Y. Y. Tu, T. Xia and L. C. Peng, *Renewable Energy*, 2020, 159, 1128–1138.

65 M. Wang, Y. X. Wang, J. Y. Liu, H. Yu, P. Liu, Y. J. Yang, D. Sun, H. Kang, Y. T. Wang, J. F. Tang, C. X. Fu and L. C. Peng, Green Carbon, 2024, 2, 164-175.

Green Chemistry

- 66 C. F. Fan, G. Y. Wang, L. M. Wu, P. Liu, J. F. Huang, X. H. Jin, G. F. Zhang, Y. P. He, L. C. Peng, K. M. Luo and S. Q. Feng, Carbohydr. Polym., 2020, 232, 115448.
- 67 Y. H. Gao, Z. P. Xu, L. J. Zhang, S. C. Li, S. G. Wang, H. L. Yang, X. L. Liu, D. Zeng, Q. Q. Liu, Q. Qian, B. C. Zhang and Y. H. Zhou, Nat. Commun., 2020, 11, 5219.
- 68 R. Zhang, H. Z. Hu, Y. M. Wang, Z. Hu, S. F. Ren, J. Y. Li, B. Y. He, Y. T. Wang, T. Xia, P. Chen, G. S. Xie and L. C. Peng, J. Exp. Bot., 2020, 71, 2956-2969.